Literature Review

Determining The Parameters of Exoplanetary Candidates From Transit Timing Variations (Working Title)

Jack Lloyd-Walters FRAS

UP881788

MSc (Honours) Degree in Physics, Astronomy, and Cosmology

School of Mathematics and Physics

2022

wordcount: 1896 words

Contents

1 Exoplanets

1.1 A brief history

While exoplanets had been thought to exist for centuries, with Giordano Bruno postulating their existence in 1584, it was not until near the turn of the twenty first century that humanity first confirmed the existence of planets beyond the solar system.

Though the first detection of an exoplanet has been retroactively pushed back to 1917 [3], the first confirmed case occurred in 1992, with the discovery of two super-terrestrial mass planets around the millisecond pulsar, PSR B1257+12 [14], due to slight anomalies in the rotation period of the pulsar.

In 1995, the first detection of an exoplanet orbiting a main sequence star was announced. 51 Pegasi-b, a hot-Jupiter orbiting it's parent star at just 7.8 million kilometres, was detected by Doppler spectroscopy [10]. This method, also known as the radial velocity method, requires the precise measurement of the radial velocity of the star as it orbits around the system barycentre, and provides extremely sensitive measurement of the planets orbital properties.

Since those first two detections, numerous telescopes have searched for exoplanets over the years, both space and ground based. Of those, arguably the most notable are the space based observatories Kepler and Tess, launched in 2009 and 2018. Between the two, they have discovered 3383 planets, with a further 6574 unconfirmed [9].

In 2016, The TRAPPIST-1 system was announced to the world, with it's close knit multi-Laplace resonance of seven terrestrial planets [6]. This marked a huge moment for current research (and my own interest in exoplanets!) owing to their many unique properties and the large scientific potential. Of the nearly five thousand exoplanets discovered, over 800 of them exist as part of a multi-planetary system like TRAPPIST-1. Planets like these, that both transit and contain multiple planets on the system, are of particular interest for this project, as I will attempt to locate additional planets in transiting systems and model them.

1.2 Transit detection

When a planet passes in front of it's parent star relative to the earth, the starlight observed is decreased by an amount proportional to the ratio of the angular area of the star and planet. This reduction in light, also called occlusion depth, provides a surprisingly powerful tool to probe the properties of exoplanets.

$$\delta = \frac{\theta_{planet}}{\theta_{star}} = \frac{R^2_{planet}}{R^2_{star}} \approx \frac{r^2_{planet}}{r^2_{star}} \tag{1}$$

A simple approximation for occlusion depth is shown in equation 1, where θ is the angular area of each object, R is the angular radius of each object, and r is the true radius of each object.

The time over which this transit occurs is a function of the planets motion, and the relative sizes between the planet and star. If we assume that the planetary motion is linear and velocity constant with respect to our vantage point, then the time period can be given as in equation 26.

$$T = 2\left(R_{star} - R_{planet}\right)/v \tag{2}$$

$$\tau = 2R_{planet}/v \tag{3}$$

$$T = t + 2\tau = 2\left(R_{star} + R_{planet}\right)/v \tag{4}$$

Where t is the time during which the planetary disk is contained completely within the stellar disk, τ is the time over which the planetary disk is only partially contained within the stellar disk (also called ingress/egress time), T is the total time during which the star is occluded, and a and v are the semi-major axis and orbital velocity of the planet. The lightcurve that would be given by this transit approximation is shown in figure 1, and the derivation and explanation for this is given in section 3.1.1.

In the case where the planet is not completely co-planar with the Earths field of view, it will instead transit above or below the centre of the disk of the star. This can be expressed in terms of the *impact parameter*, b of the transit [8], as given in equation 5.

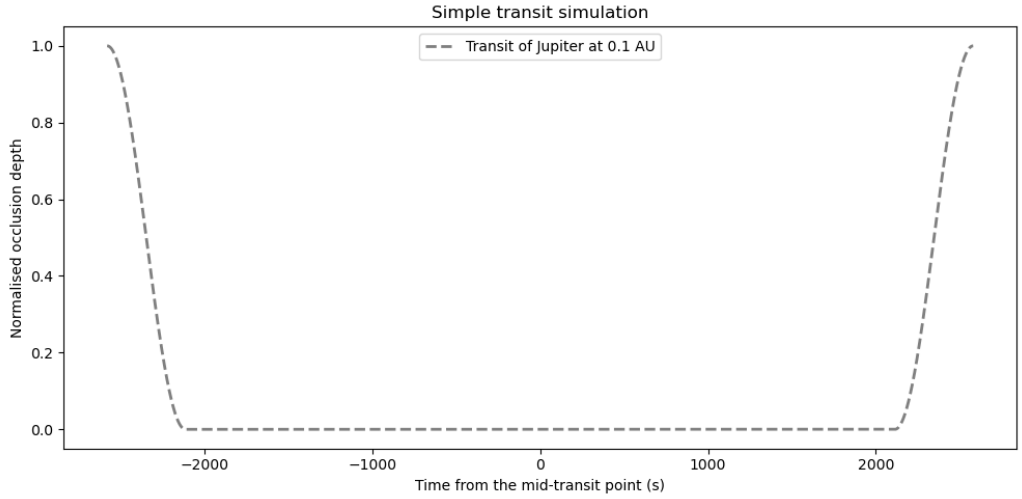

Figure 1: A simple transit simulation of Jupiter situated 0.1AU from the sun.

$$b = \frac{a\cos(i)}{R_{star}} \tag{5}$$

Where a and i are the semi-major axis and relative inclination of the orbit. This offset from the centre of the star also slightly modifies the transit time [13], as shown in equation 7, with the derivation and explanation given in section 3.1.2.

$$l_T = \sqrt{(R_{star} + R_{planet})^2 - (bR_{star})^2} \tag{6}$$

$$T = \frac{2a}{v}\arcsin\left(\frac{\sqrt{(R_{star} + R_{planet})^2 - (bR_{star})^2}}{a}\right) \tag{7}$$

The transiting timing recovered from this equation provides a solid baseline with which to plan future observations of my target planetary systems, such that our entire observation window is long enough to include the entire transit.

2 Transit Timing Variation

Transit timing variation occur when a planet transits its parent star at different intervals than predicted from integrating the planets motion with a simple 2-body model. A number of factors can cause this, with the primary notes of interest being perturbation effects of additional planets in the system. Using this method to locate other planets is a relatively recent idea, first postulated in 2005 [1], with additional papers in 2007 [7].

A number of planets have been detected this way [11] [2] [12], two of which are candidate targets for this research project, due to their being deep transits that should display measurable variation.

2.1 The science

Loosely speaking, there are two primary causes for planet-caused transit timing variations, those being the relative motion of the entire system as the centre of mass shifts, and the changing of orbital parameters as a result of n-body dynamics.

2.1.1 Motion of the Barycentre

All bodies in a system orbit about a common centre of mass, or the global barycentre of the system. The motion of additional planets in the system causes this global barycentre to move relative to the position of the local barycentre between the star and transit target. This motion results in the orbit of the transit planet oscillating, and thus transits will appear to lead or lag the time given by a simple 2-body Keplerian orbit.

$$r_p = \frac{am_s}{m_p + m_s} = a - r_s \tag{8}$$

Equation 8 gives the distance between the barycentre and the primary r_p as a function of the mass of the primary and secondary m_p, m_s and the semi-major axis of the orbit about the primary a.

The motion of the barycentre along a single axis for each planet individu-

ally can be given as a simple sinusoidal function. The motion of the global barycentre can thus be given by the summation of the individual components, as shown in equation 9.

$$d_{global} = \sum_{i}^{n} (d_i) = \sum_{i}^{n} (r_i \sin(2\pi t/T_i)) \tag{9}$$

Where d is the location of each barycentre along this axis, r_i is the distance between the central body and each local barycentre, and T_i is the orbital period of each orbiting body.

If we consider the case where two planets are in circular orbits with a simple 2:1 resonance, and their masses are such that the outer planet contributes half as much to the global barycentre as the central planet does, then the combined motion of the global barycentre along an axis perpendicular to our field of view can be given in equation 10

$$d_{global} = \sin(2\pi t) + 0.5 \sin(2\pi t/2) \tag{10}$$

This provides two distinct points per synodic period. Where the planets are aligned, the transit will appear earlier than expected, while the planets being anti-aligned will cause the transit to appear later than expected, as shown in figure 2. This motion is the primary cause for transit timing variation, and is what I will be attempting to measure with my own observation, and subsequent search code.

2.1.2 Perturbation of the Orbit

In the case where planets orbit distantly enough, and have low enough masses, then the orbital motion of each body in the system can be very well approximated by Keplerian orbits. This approximation, however, requires the introduction of perturbation terms in the case where the gravitational interaction between planets in the system is significant.

In the case where bodies in the system are distant, the n-body interactions will cause apsidal precession, in which the argument of periapse will change over time, as shown in figure 3. These interactions are the dominant cause

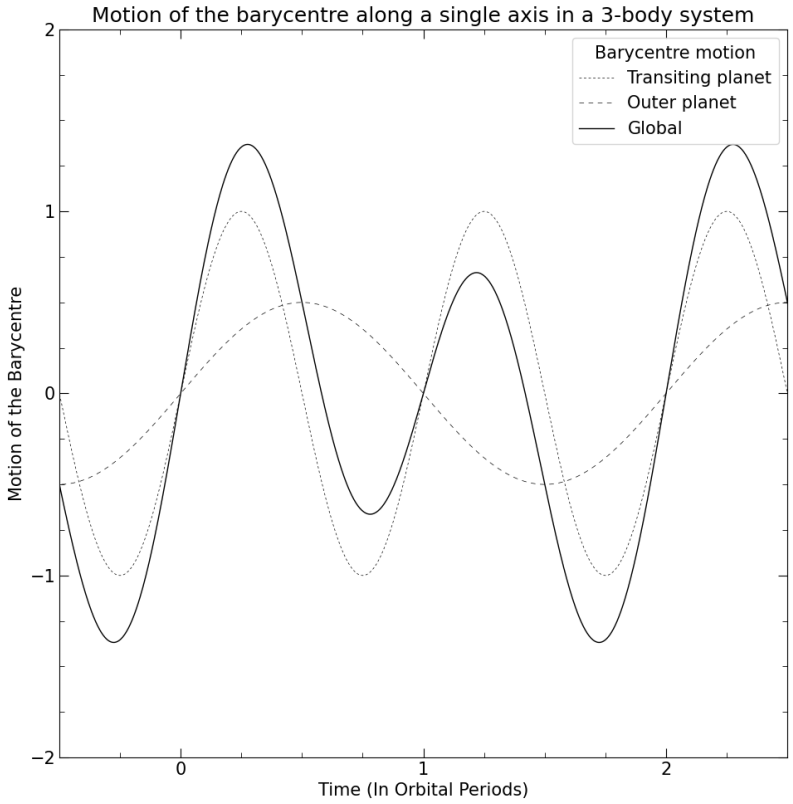

Figure 2: The motion of the barycentre as it evolves over time. As this is a simple circular 2:1 resonance, the oscillations occur over the synodic timescale of twice the orbital period of the central body.
As the divergence between the 2-body and global barycentric motion is entirely dependent on the motion of the outermost planet in this case, the measurement of transit timing variation would allow the recovery of information on the barycentric parameter (mass $*$ semi-major axis) of the outer planet from simple Fourier analysis.

of apsidal precession in the solar system [4], and are expected to be similar in multi-exoplanetary systems too.

Apsidal precession causes a near constant increase in the period between transits as a result of the argument of periapse of the orbit rotating relative to earth. As a result of this, the true anomaly of the orbit at which each transit occurs changes over time, slightly changing both the width and depth of each transit due to the slight variations in orbital velocity and instantaneous orbital radius over the entirety of the orbit.

$$T_P = \frac{a_P}{a} + 2\cos(i)\sqrt{\left(\frac{a}{a_P}\left(1-e^2\right)\right)} \tag{11}$$

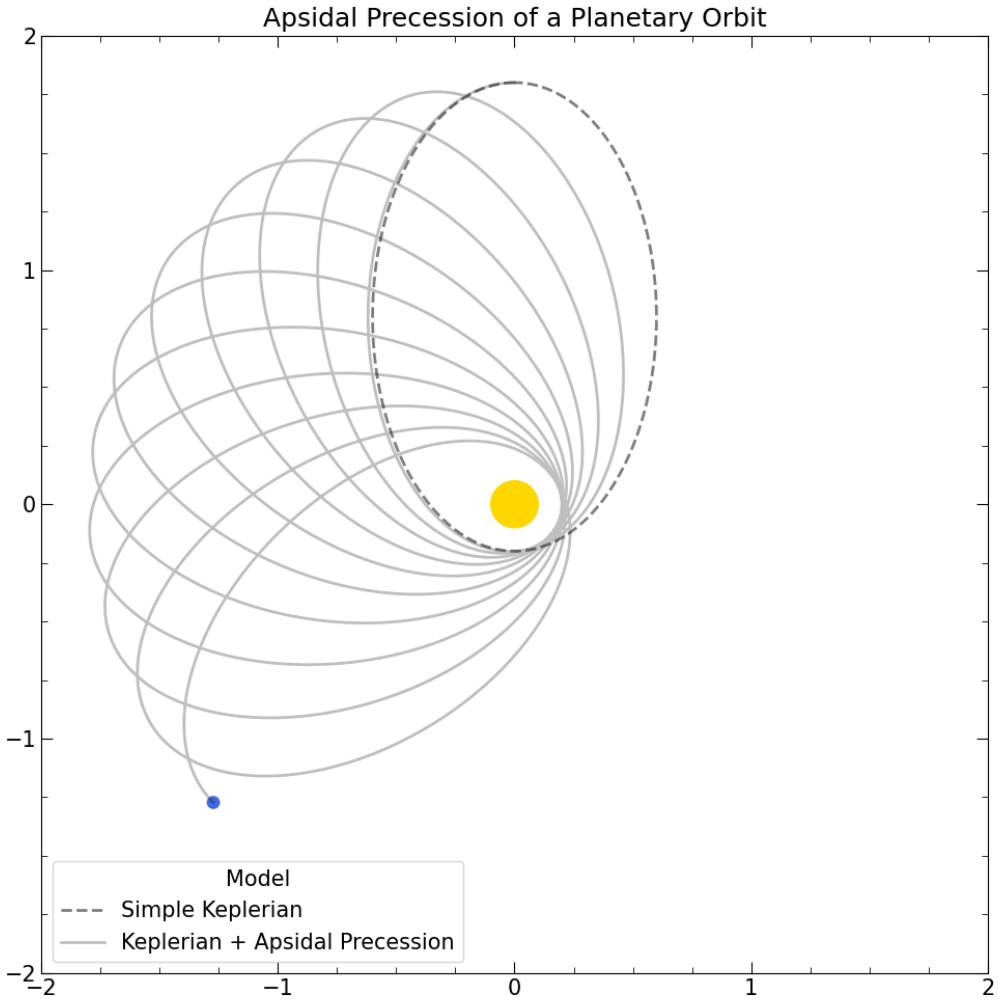

Figure 3: The argument of periapse of a planet changes over time as a result of perturbation.

Apsidal precession, however, is not the only effect when planetary orbits are close. The quasi-conserved quantity of gravitational interactions, the Tisserand parameter T_P [5], is given in equation 11, and relates the semi-major axis a, orbital eccentricity e, and inclination i of a primary body to that of a secondary perturbing body with semi-major axis a_p.

An extreme example of this in our own solar system is the co-orbital motion of the Saturnian moons Janus and Epimethius, a dynamically stable system in which the moons effectively swap orbits, which causes transits of the moons across Saturn to vary over time.

As a result of the Tisserand parameter, perturbations can cause dynamically stable resonances between any of semi-major axis, eccentricity, and inclination to occur over geological time. A specific named example is the Kozai mechanism, as shown in equation 12, where the inclination and eccentricity of a perturbed body will oscillate over a timescale as defined by equation 13.

$$L_z = \sqrt{1 - e^2}\cos(i) = \text{constant} \tag{12}$$

$$T_k = \frac{P_2^2}{P}\left(1 - e_2^2\right)^{3/2} \tag{13}$$

Where P and e are the orbital period and eccentricity, and subscript 2 denotes the properties belong to the perturbing planet. As both eccentricity and inclination determine the timing and depth of a transit event, a secondary perturbing body with large co-inclination could potentially be found from transit variations of the primary body, even when the perturbing body could never be observed by transit method itself.

2.2 Alternatives

Unfortunately, perturbations by additional planets in the system are not the only mechanisms by which a planets true orbit diverges from it's osculating one, and need to be taken into account when looking for any potential TTV's caused by planets with my search code.

2.2.1 Non-spherical central body

In the case where the central body has a non-spherical geometry, as is to be expected from a rotating star, for example, the resulting gravitational field will also be non-spherical. An object that orbits an oblate central body will exhibit nodal precision: as the Equatorial bulges attempt to drag the orbital inclination into the plane of rotation, the orbit is twisted around the central body due to gyroscopic deflection.

$$\omega_p = -\frac{3}{2}\frac{R^2}{\left(a\left(1 - e^2\right)\right)^2} J_2 \omega \cos i \tag{14}$$

$$J_2 = \frac{2\varepsilon}{3} - \frac{R^3\omega_b^2}{3\mu} \tag{15}$$

The rate of nodal precession, ω_p is given in equation 14, where a, e, i, ω are the semi-major axis, eccentricity, inclination, and angular velocity of the satellites orbit, R is the equatorial radius of the central body, and J_2 is a quantity that relates the oblateness of the central body from the geopotential model of the body, which is given in equation 15, where ε, ω_b, and μ is the oblateness, rotation rate, and gravitational parameter of the central body.

An example of this usage is the sun synchronous orbit, where the nodal precession from the earths non-spheroidal shape is used to twist the satellites orbit at the same rate that the earth orbits the sun, keeping the sun at a fixed location relative to the satellite. In the case of an exoplanet, this is presumed to have minimal consequence.

2.2.2 Relativity

A far more significant divergence from simple Keplerian orbits that we expect to see among many transiting exoplanets is the apsidal precession caused by general relativity, give in equation 16.

$$\varepsilon = 24\pi^3 \frac{a^2}{Pc^2(1-e^2)} \tag{16}$$

Where ε is the apsidal precession per orbital revolution, and c is the speed of light. The introduction of the speed of light term squared on the denominator evidently demonstrates that this effect is small, but non-negligible, as we have seen the 43 arc-second precession of mercury over the last century. This effect changes the transit properties identically to other orbiting bodies, though with differing magnitudes heavily dependent on the semi-major axis.

2.2.3 Natural Satellites

In much the same way that additional planets can move the global barycentre of the system, Exo-moons will cause their parent planet to oscillate about their own common barycentre too [8]. This effect should cause smaller variations than those caused by other planets in the system, and have yet to

be observed, but could still potentially cause additional TTV outside of the focus of this project.

3 Appendix

3.1 Derivation and Explanation of Equations

3.1.1 Transit length in the linear approximation

If we assume that the planets orbit is large, compared to the distance it travels in an orbit, then we can approximate the path the planet takes in front of its parent star as a line segment.

We know the orbital velocity of a body from the vis-viva equation, where μ is the gravitational parameter, r the radial distance between the bodies, and a the semi-major axis of the orbit.

$$v^2 = \mu\left(\frac{2}{r} - \frac{1}{a}\right) \tag{17}$$

The radial distance, r, can either be measured from the transit, or, if a model of the orbit is known, recovered from the true anomaly ν and eccentricity e as given below.

$$r = a\frac{1 - e^2}{1 + e\cos\nu} \tag{18}$$

As we know the transit path is small compared to the orbit, we also know that r will change negligibly over this path, and thus v^2 remains constant. Additionally, if the eccentricity of the orbit is small, then $r \approx a$ as seen from equation 18, and the vis-viva equation simplifies to the form provided.

$$v^2 \approx \frac{\mu}{r} \tag{19}$$

If we have constant velocity, we can utilise simple laws of motion, such as $v = t/s$, to recover the crossing time:

$$t_{transit} = v_{transit}s_{transit} \tag{20}$$

where $t_{transit}$ is the time over which the transit occurs, $v_{transit}$ is the velocity of the body during the transit, and $s_{transit}$ is the distance that the body covers.

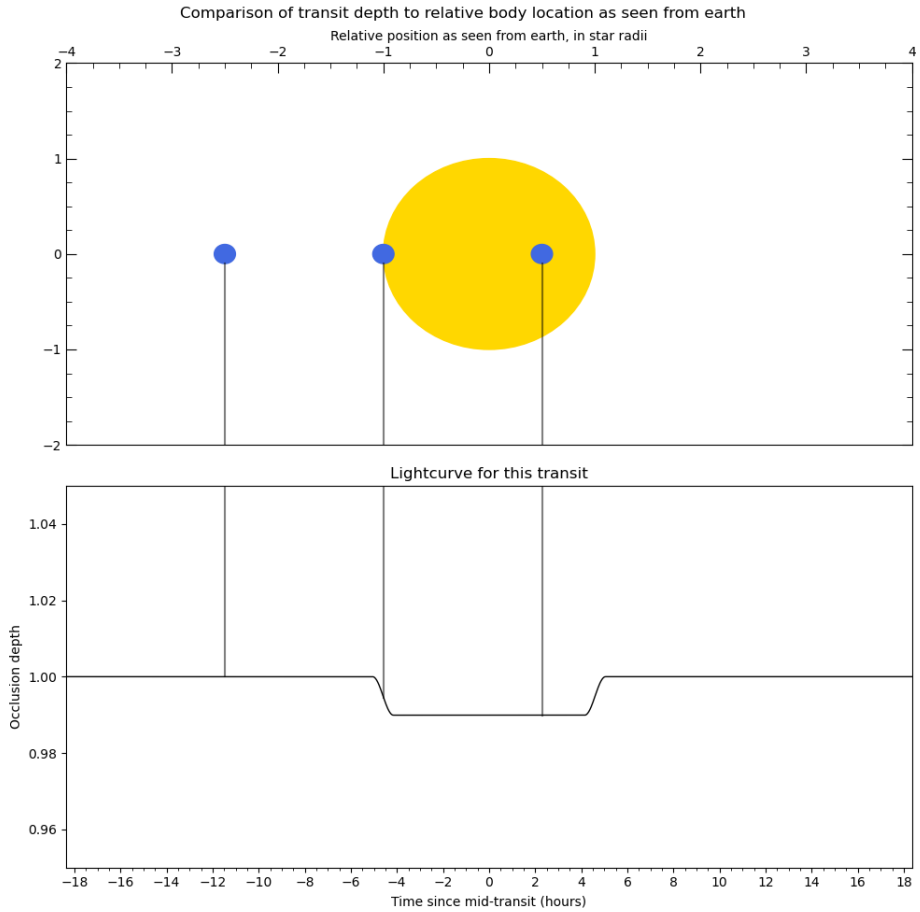

Figure 4: The top graph shows the planet position, with lines joining the second chart, which shows the corresponding lightcurve at that planets position.

As we can see from figure 4, the planetary transit reaches maximum occlusion when the planet is completely covered by the star, and has a transition period when only partially bounded. The exact depth of the transit can be found by considering the intersection of two circles, but is not a part of this derivation.

The transit will begin when the planet first begins to occlude the star, which we can see from figure 4, thus the centre of the planet will be a distance from the centre of the star equal to the sum of their radii. The full occlusion transit will occur when the planet has moved a distance equal to it's diameter

compared to the full transit.

Thus, we have expressions for the distance for the full transit, $s_{transit}$, the transitional period $s_{transition}$, and the full occlusion $s_{occluded}$.

$$s_{occluded} = 2\left(R_{star} - R_{planet}\right) \tag{21}$$

$$s_{transition} = 2\left(R_{planet}\right) \tag{22}$$

$$s_{transit} = s_{occluded} + s_{transition} = 2\left(R_{star} + R_{planet}\right) \tag{23}$$

We can finally resolve the time through which the transit will occur, using the simple $t = s/v$, as given in equation 26, which completes our derivation for equation 4.

$$t = 2\left(R_{star} - R_{planet}\right)/v \tag{24}$$

$$\tau = 2\left(R_{planet}\right)/v \tag{25}$$

$$T_{transit} = t + \tau = 2\left(R_{star} + R_{planet}\right)/v \tag{26}$$

3.1.2 Transit Length for an inclined orbit

For a planet in an inclined orbit, parts of the transit will occur off-centre from the parent star. As such, while the previous assumption that the transit is small compared to the orbit holds, then assumption that the transit appears *linear* is slightly incorrect.

This can be demonstrated with figure 5, though the effect is subtle, the orbits are most definitely not quite linear.

An additional property of a transit can be used to describe this system. The so called "Impact parameter" defines the offset of the centre of the transit due to orbital inclination, and is given in equation 27 below.

$$b = \frac{a\cos i}{R_{star}} \tag{27}$$

Where b is the impact parameter, and a and i are the semi major axis and relative inclination of the orbit. The parameter is computed from simple

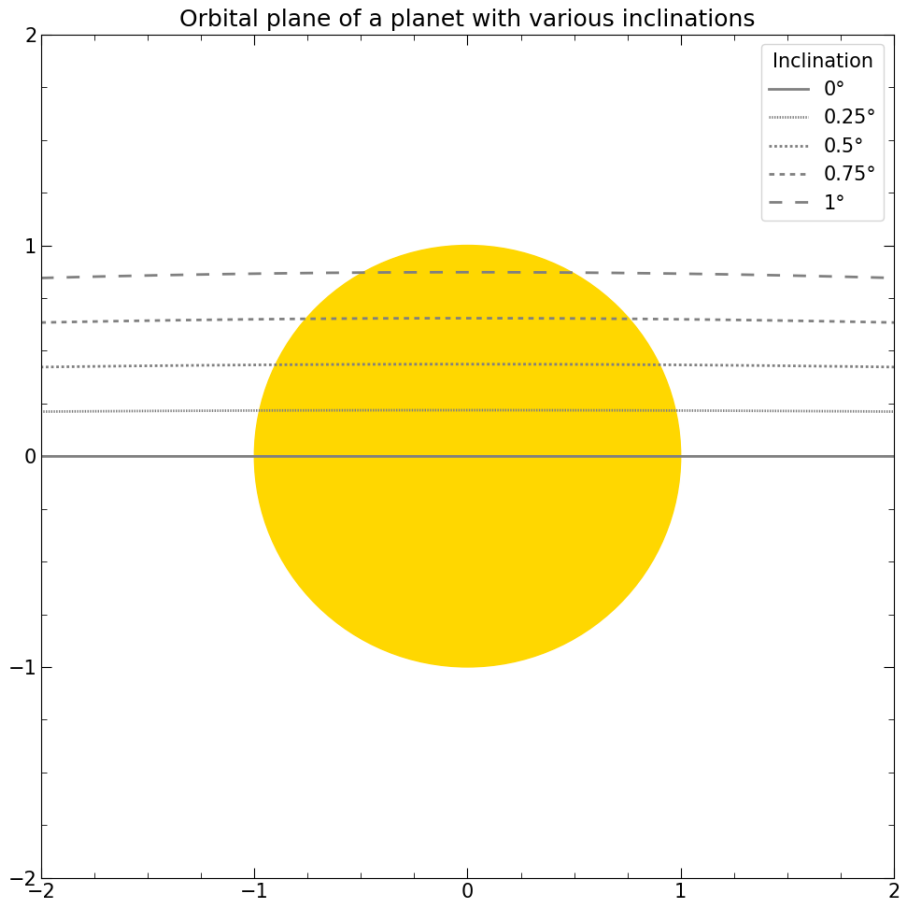

Figure 5: Comparison between equatorial and inclined orbits. The different lines show orbits of differing relative inclinations. Note the increasing non-linearity as the relative inclination grows.

trigonometry, and normalised to the stars radius, such that $b = 1$ defines the orbit as crossing directly at the stars radius.

Additionally, the relative inclination is defined such that $i = 90°$ is edge-on from the vantage point of the earth. As we can see from 6, the impact parameter is defined in the case where the ascending node of the orbit is aligned perpendicular to earth. A slight extension is required for other Longitude of ascending nodes, given in equation 28.

$$b = \frac{a \cos i}{R_{star}} \sin \Omega \tag{28}$$

Where Ω is the Longitude of ascending node, defined such that $\Omega = 0$

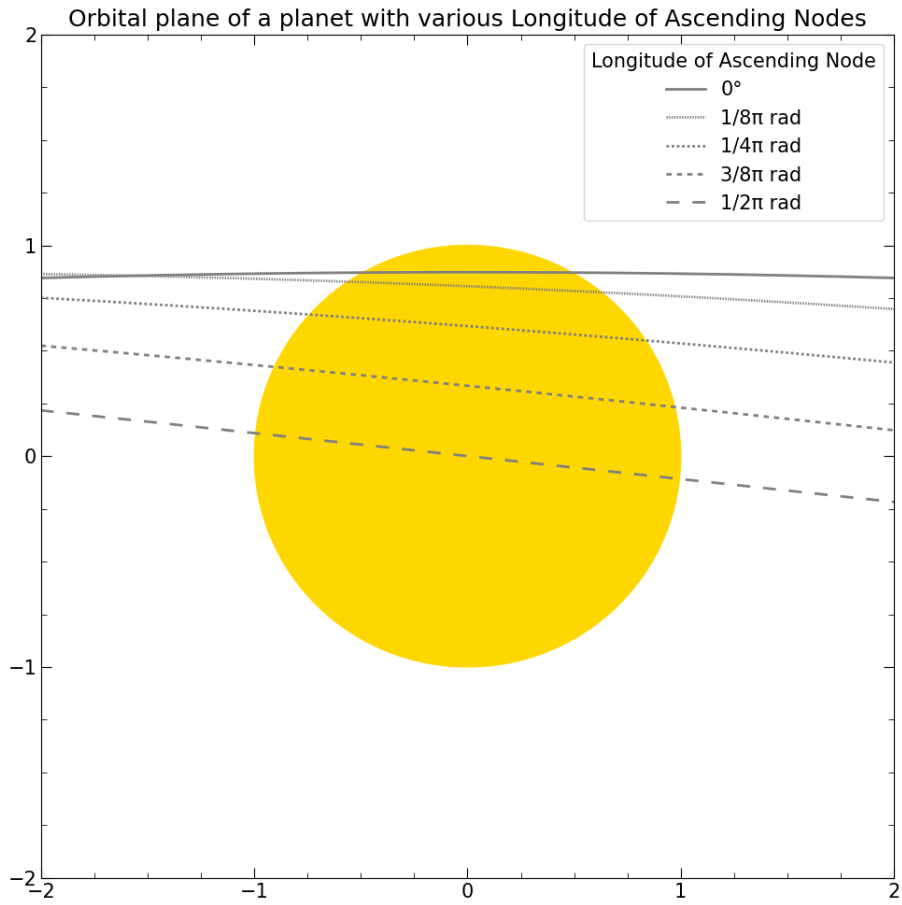

Figure 6: Comparison between various ongitude of periapsis. The different lines show orbits with the same inclination, but with different longitude of ascending nodes. Note how the orbit becomes more linear as the descending node approaches the centre of the star.

is perpendicular to the line of sight of earth, and simplifies to our previous expression for b.

The total distance the planet covers during the course of its transit is twice that swept by the angle β in figure 7, which is simply a circle arc, and is given by:

$$s = 2\beta a \tag{29}$$

Figuring out β is not exactly trivial, though we do know it must occur such that the planet is just about to transit the star, as mentioned in the above section. Thus, we know that the radial distance from the planet and star's

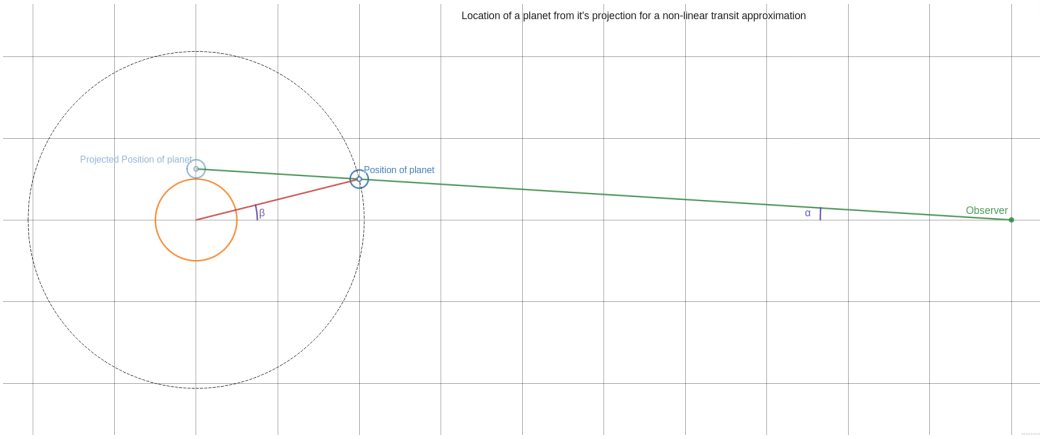

Figure 7: Geometry of a non-linear transit. The projection of the planet compared to it's actual position, as well as the angles between itself, the observer, and the star, are visible.

centres must be $r = r_{planet} + r_{star}$. The projected position of the planet at the beginning of the transit must also be aligned with the impact parameter, such that the linear distance from the line of sight to the end of the transit is:

$$R_\beta = \sqrt{(R_{star} + R_{planet})^2 - (bR_{star})^2} \tag{30}$$

We can thus recover β from simple trigonometry, specifically the identity $\sin\theta = opposite/hypotenuse$:

$$\sin\beta = \frac{R_\beta}{a} = \frac{\sqrt{(R_{star} + R_{planet})^2 - (bR_{star})^2}}{a} \tag{31}$$

and can combine with equation 29 to give the transit distance:

$$s = 2\beta a = 2a \arcsin\left(\frac{R_\beta}{a}\right) \tag{32}$$

For which we can finally introduce the orbital velocity to obtain the transit time equation 33, and have shown the derivation for equation 7.

$$T = \frac{2a}{v} \arcsin\left(\frac{R_\beta}{a}\right) \tag{33}$$

3.2 Project Proposal

3.2.1 Summarised plan

The overarching goal of this project is to determine whether any exoplanets exhibit transit timing variations, and attempt to measure that variation using a mix of historical data and observations that I will carry out over the course of this project.

My own observations will be made with the 24" Ritchey-Chrétien telescope at Clanfield observatory, and analysed using the HOPS software maintained by Exoworldspies. This software will allow me to determine properties of the transit, such as occlusion depth and transit period, that can inform my understanding of the physical parameters of the system. I will also upload my own observations to the Exoclock website, to expand upon historical ephemeris data.

Transit timing variations will be extracted from historical lightcurve data using a set of python scripts that I will write over the course of this project. If transit timing variations are found for any systems, I will attempt to determine the parameters of additional planets within the system and so derive a model of the system. This solution can be compared against both n-body simulation and published literature to determine the accuracy of my model.

3.2.2 Observation target selection

To narrow down the thousands of exoplanet systems to something more feasible, a query was made to the NASA Exoplanet Archive for planets that matched the following criterion:

- The system contains a single star, and at least two planets.
- At least one of the planets was discovered by Transit method.
- The system must have Right Ascension between 4h and 15h. This places it 6.5 hours either side of the Sun (as of 2022-02-07), and ensures the planet is visible at night time.
- The system must have declination greater than zero.

- The central Star must have a visual magnitude smaller than 15.

There were 85 planetary candidates returned by this query. Of those 85, 23 were also listed in the exoclock database, and are summarised in table 1.

Of the initial 85 candidates, 7 were flagged in the exoplanet archive as exhibiting Transit timing variations, shown in table 2.

Name	Observations ExoClock / ETD	Right Ascension hh:mm:ss	Declination dd:mm:ss	Visual Magnitude mag	Transit Depth mmag
HAT-P-13 b	11 / 109	08:39:31.81	+47:21:07.26	10.40	8.25
HAT-P-44 b	10 / 43	14:12:34.57	+47:00:53.05	12.83	24.45
HD 63433 b	0 / 0	07:49:55.06	+27:21:47.46	6.49	0.62
HD 63433 c	0 / 0	07:49:55.06	+27:21:47.46	6.49	0.90
HD 63935 b	0 / 0	07:51:41.99	+09:23:09.79	8.10	1.02
HD 63935 c	0 / 0	07:51:41.99	+09:23:09.79	8.10	0.08
HIP 41378 e	0 / 0	08:26:27.85	+10:04:49.33	8.62	1.71
HIP 41378 f	0 / 0	08:26:27.85	+10:04:49.33	8.62	5.72
K2-18 b	0 / 0	11:30:14.52	+07:35:18.26	13.24	3.49
K2-19 b	0 / 0	11:39:50.48	+00:36:12.88	12.88	7.63
K2-19 c	0 / 0	11:39:50.48	+00:36:12.88	12.88	2.55
K2-36 c	0 / 0	11:17:47.78	+03:51:59.01	11.48	1.6
K2-155 c	0 / 0	04:21:52.48	+21:21:12.94	12.46	1.39
K2-239 b	0 / 0	10:42:22.63	+04:26:28.89	14.14	0.86
KELT-6 b	2 / 1	13:03:55.65	+30:38:24.28	10.00	7.89
TOI 561 b	0 / 0	09:52:44.55	+06:12:58.92	9.78	0.31
TOI 561 c	0 / 0	09:52:44.55	+06:12:58.92	9.78	1.27
TOI 1266 c	0 / 0	13:11:59.56	+65:50:01.70	12.58	1.44
TOI 2076 b	0 / 0	14:29:34.24	+39:47:25.54	8.66	2.06
V1298 Tau b	0 / 0	04:05:19.59	+20:09:25.56	9.57	6.29
V1298 Tau c	0 / 0	04:05:19.59	+20:09:25.56	9.57	1.93
V1298 Tau d	0 / 0	04:05:19.59	+20:09:25.56	9.57	2.56
V1298 Tau e	0 / 0	04:05:19.59	+20:09:25.56	9.57	4.67

Table 1: List of planetary candidates that are in the Exoclock Database alongside the number of transit observations that have been recorded in both Exoclock and the Exoplanetary Transit Database. Exoplanets are coloured where their transit depth exceeds 5mmag (dark blue), 10mmag (blue), or 20mmag (light blue).
Data taken from ExoClock.

Name	Right Ascension	Declination	Visual Magnitude
	hh:mm:ss	dd:mm:ss	mag
HAT-P-13 b	08:39:31.77	+47:21:06.87	10.421
HIP 41378 c	08:26:27.80	+10:04:49.33	8.930
K2-19 b	11:39:50.46	+00:36:12.95	13.024
K2-19 c	11:39:50.46	+00:36:12.95	13.024
K2-19 d	11:39:50.46	+00:36:12.95	13.024
TOI-1266 b	13:11:59.18	+65:50:01.31	12.941
TOI-1266 c	13:11:59.18	+65:50:01.31	12.941

Table 2: List of planetary candidates that were flagged as exhibiting transit timing variation. Data taken from Nasa Exoplanet Archive.

3.2.3 Observational Windows

Observational windows in February, March, and April for observable planet of interest is given in table 3. This table includes both the start and end times of the transit event, as well as the observation window which includes an hour before and after the transit.

Table 4 shows a shortlist of 9 proposed observations to be considered for telescope time.

Name	Source	Observation Start	Transit Start	Transit End	Observation End
HAT-P-13 b	Exoclock	2022-02-19 00:37	2022-02-19 01:37	2022-02-19 04:56	2022-02-19 05:56
HAT-P-44 b	Exoclock	2022-02-21 21:56	2022-02-21 22:56	2022-02-22 03:09	2022-02-22 04:09
HAT-P-13 b	Exoclock	2022-02-21 22:37	2022-02-21 23:37	2022-02-22 02:56	2022-02-22 03:56
HAT-P-13 b	Exoclock	2022-02-24 20:36	2022-02-24 21:36	2022-02-25 00:56	2022-02-25 01:56
HAT-P-13 b	Exoclock	2022-02-27 18:36	2022-02-27 19:36	2022-02-27 22:55	2022-02-27 23:55
HAT-P-44 b	Exoclock	2022-03-06 19:37	2022-03-06 20:37	2022-03-06 23:49	2022-03-07 00:49
K2-19 b	Exoclock	2022-03-09 22:34	2022-03-09 23:34	2022-03-10 03:03	2022-03-10 04:03
K2-19 b	Exoclock	2022-03-17 20:38*	2022-03-17 21:38*	2022-03-18 01:07*	2022-03-18 02:07*
KELT-6 b	ETD	2022-03-19 23:55*	2022-03-20 00:55*	2022-03-20 06:26*	2022-03-20 07:26*
HAT-P-44 b	Exoclock	2022-03-24 00:31	2022-03-24 01:31	2022-03-24 04:44	2022-03-24 05:44
K2-19 b	Exoclock	2022-03-25 18:42	2022-03-25 19:42	2022-03-25 23:11	2022-03-26 00:11
KELT-6 b	Exoclock	2022-03-27 19:39	2022-03-27 20:39	2022-03-28 02:31	2022-03-28 03:31
HAT-P-13 b	Exoclock	2022-03-28 22:33	2022-03-28 23:33	2022-03-29 02:52	2022-03-29 03:52
HAT-P-13 b	Exoclock	2022-03-31 20:33	2022-03-31 21:33	2022-04-01 00:52	2022-04-01 01:52
HAT-P-13 b	ETD	2022-04-03 18:38	2022-04-03 19:38	2022-04-03 22:51	2022-04-03 23:51
KELT-6 b	ETD	2022-04-04 16:30	2022-04-04 17:30	2022-04-04 23:01	2022-04-05 00:01
HAT-P-44 b	Exoclock	2022-04-05 22:13	2022-04-05 23:13	2022-04-06 02:25	2022-04-06 03:25
HAT-P-44 b	Exoclock	2022-04-18 19:54*	2022-04-18 20:54*	2022-04-19 00:07*	2022-04-19 01:07*

Table 3: Observational windows for planets with TTV flags or transit depths greater than 5mmag, where dates marked with an asterisk occur within two days of the full moon
Times marked in red occur too late at night for consideration, while planets marked in orange indicate observations that require pointing the telescope north or north east, and require assessing the risk of the telescope impacting its mount.
Times marked with a yellow background indicate that the sun is in the sky.

Name	Source	Observation Start	Transit Start	Transit End	Observation End
HAT-P-13 b	Exoclock	2022-02-24 20:36	2022-02-24 21:36	2022-02-25 00:56	2022-02-25 01:56
HAT-P-13 b	Exoclock	2022-02-27 18:36	2022-02-27 19:36	2022-02-27 22:55	2022-02-27 23:55
HAT-P-44 b	Exoclock	2022-03-06 19:37	2022-03-06 20:37	2022-03-06 23:49	2022-03-07 00:49
K2-19 b	Exoclock	2022-03-17 20:38*	2022-03-17 21:38*	2022-03-18 01:07*	2022-03-18 02:07*
K2-19 b	Exoclock	2022-03-25 18:42	2022-03-25 19:42	2022-03-25 23:11	2022-03-26 00:11
HAT-P-13 b	Exoclock	2022-03-31 20:33	2022-03-31 21:33	2022-04-01 00:52	2022-04-01 01:52
HAT-P-13 b	ETD	2022-04-03 18:38	2022-04-03 19:38	2022-04-03 21:51	2022-04-03 23:51
KELT-6 b	ETD	2022-04-04 16:30	2022-04-04 17:30	2022-04-04 23:01	2022-04-05 00:01
HAT-P-44 b	Exoclock	2022-04-18 19:54*	2022-04-18 20:54*	2022-04-19 00:07*	2022-04-19 01:07*

Table 4: A shortlist of proposed telescope observations is given. The same colour formatting applies as in table 3.

Week beginning	deadlines	Transits	Progress checkpoints
2022-02-07			Collect related scientific papers
2022-02-14			
2022-02-21		2 x HAT-P-13 b	Lit. review draft
2022-02-28	Lit. review	HAT-P-44 b	Poster draft
2022-03-07	Poster submission		start writing code
2022-03-14	Poster presentation	K2-19 b	
2022-03-21		K2-19 b	
2022-03-28		2 x HAT-P-13 b	Initial TTV search code complete
2022-04-04		KELT-6 b	
2022-04-11			
2022-04-18		HAT-P-44 b	
2022-04-25			Final iteration of TTV search code complete
2022-05-02			presentation draft
2022-05-09	Presentation submission		
2022-05-16	Deliver oral presentation		Final dissertation draft
2022-05-23	Dissertation submission		

Table 5: A rough approximation of the schedule required for this project

3.2.4 Timescale

The project will take place over the next three months, with a rough timeline given in table 5. Included are required deadlines, any transits from table 4, and ideal progress to have made by the end of that week. As with any rough timeline, this will no doubt be subject to change as different occurrences happen.

3.3 Bibliography

[1] Eric Agol et al. "On detecting terrestrial planets with timing of giant planet transits". In: *Monthly Notices of the Royal Astronomical Society* 359.2 (2005-05), pp. 567–579. ISSN: 0035-8711. DOI: 10.1111/j.1365-2966.2005.08922.x. eprint: https://academic.oup.com/mnras/article-pdf/359/2/567/3098498/359-2-567.pdf. URL: https://doi.org/10.1111/j.1365-2966.2005.08922.x.

[2] Sarah Ballard et al. "THE KEPLER-19 SYSTEM: A TRANSITING 2.2R⊕PLANET AND A SECOND PLANET DETECTED VIA TRANSIT TIMING VARIATIONS". In: *The Astrophysical Journal* 743.2 (2011-12), p. 200. DOI: 10.1088/0004-637x/743/2/200. URL: https://doi.org/10.1088/0004-637x/743/2/200.

[3] J. Farihi. "Circumstellar debris and pollution at white dwarf stars". In: *New Astronomy Reviews* 71 (2016-04), pp. 9–34. ISSN: 1387-6473. DOI: 10.1016/j.newar.2016.03.001. URL: http://dx.doi.org/10.1016/j.newar.2016.03.001.

[4] Richard Fitzpatrick. *Perihelion Precession of the Planets*. 2013. URL: https://farside.ph.utexas.edu/teaching/336k/Newtonhtml/node115.html (visited on 2022-02-19).

[5] Richard Fitzpatrick. *Tisserand Criterion*. 2011. URL: https://farside.ph.utexas.edu/teaching/336k/Newtonhtml/node122.html (visited on 2022-02-20).

[6] Michaël Gillon et al. "Temperate Earth-sized planets transiting a nearby ultracool dwarf star". In: *Nature* 533.7602 (2016-05), pp. 221–224. ISSN: 1476-4687. DOI: 10.1038/nature17448. URL: http://dx.doi.org/10.1038/nature17448.

[7] Jeremy S. Heyl and Brett J. Gladman. "Using long-term transit timing to detect terrestrial planets". In: *Monthly Notices of the Royal Astronomical Society* 377.4 (2007-05), pp. 1511–1519. ISSN: 0035-8711. DOI: 10.1111/j.1365-2966.2007.11697.x. eprint: https://academic.oup.com/mnras/article-pdf/377/4/1511/3796883/mnras0377-1511.pdf. URL: https://doi.org/10.1111/j.1365-2966.2007.11697.x.

[8] David M. Kipping. "Transit timing effects due to an exomoon – II". In: *Monthly Notices of the Royal Astronomical Society* 396.3 (2009-06), pp. 1797–1804. ISSN: 0035-8711. DOI: 10.1111/j.1365-2966.2009.14869.x. eprint: https://academic.oup.com/mnras/article-

pdf/396/3/1797/5804196/mnras0396-1797.pdf. URL: https://doi.org/10.1111/j.1365-2966.2009.14869.x.

[9] *List of planets detected by Kepler and TESS*. 2022. URL: https://exoplanetarchive.ipac.caltech.edu/docs/counts_detail.html (visited on 2022-02-17).

[10] Michel Mayor and Didier Queloz. "A Jupiter-mass companion to a solar-type star". In: *Nature* 378.6555 (1995-11), pp. 355–359. DOI: 10.1038/378355a0.

[11] V. Nascimbeni et al. "TASTE II. A new observational study of transit time variations in HAT-P-13b". In: *American Astrophysical Society* 532, A24 (2011-08), A24. DOI: 10.1051/0004-6361/201116830. arXiv: 1105.4603 [astro-ph.EP].

[12] Jason H. Steffen et al. ""Transit timing observations from Kepler – III. Confirmation of four multiple planet systems by a Fourier-domain study of anticorrelated transit timing variations"". In: *Monthly Notices of the Royal Astronomical Society* 421.3 (2012-04), pp. 2342–2354. ISSN: 0035-8711. DOI: 10.1111/j.1365-2966.2012.20467.x. eprint: https://academic.oup.com/mnras/article-pdf/421/3/2342/17331710/mnras0421-2342.pdf. URL: https://doi.org/10.1111/j.1365-2966.2012.20467.x.

[13] paul anthony wilson. *The exoplanet transit method*. 2016. URL: https://www.paulanthonywilson.com/exoplanets/exoplanet-detection-techniques/the-exoplanet-transit-method/ (visited on 2022-02-20).

[14] A. Wolszczan and D. A. Frail. "A planetary system around the millisecond pulsar PSR1257 + 12". In: *Nature* 355.6356 (1992-01), pp. 145–147. DOI: 10.1038/355145a0.

3.4 List of Figures